The Nature of the 660-Kilometer Upper-Mantle Seismic Discontinuity from Precursors to the *PP* Phase

Charles H. Estabrook* and Rainer Kind†

Global Seismic Network data were used to image upper-mantle seismic discontinuities. Stacks of phases that precede the *PP* phase, thought to be underside reflections from the upper-mantle discontinuities at depths of 410 and 660 kilometers, show that the reflection from 410 kilometers is present, but the reflection from 660 kilometers is not observed. A continuous Lamé's constant λ and seismic parameter at the 660-kilometer discontinuity explain the missing underside *P* reflections and lead to a *P*-wave velocity jump of only 2 percent, whereas the *S*-wave velocity and density remain unchanged with respect to previous global models. The model deemphasizes the role of Lamé's constant λ with regard to the shear modulus and constrains the mineralogical composition across the discontinuity.

Upper-mantle structure is inferred predominantly from seismic observations. Conversions from *P* to *S* waves (*1*, *2*) and reflected *P* and *S* waves (*3*–*6*) are used in the identification of the upper-mantle discontinuities. The seismic discontinuity at a depth of ~410 km (410) is associated with the phase transition of olivine to β-spinel (*7*). There is no general agreement, however, about the nature of the second major discontinuity, at a depth of ~660 km (660). Recent studies (*7*–*9*) suggest that the 660 is caused by a phase change in which γ-spinel (Sp) → perovskite (Pv) + magnesiowüstite (Mw) and garnet (Gr) → Pv; however, depending on the upper-mantle mineralogical model, the amount of olivine varies between 40% [piclogite model (*8*)] and 60% [pyrolite (*9*)]. Although the reaction Sp → Pv + Mw occurs over a narrow interval (<4 km), Gr → Pv may have a broadening effect because it would occur over a wider depth interval (*7*). The dominant reaction is thought to be Sp → Pv + Mw because observations of short-period precursors to *P′P′* (*10*) suggest that the 660 is sharp (≤4 km in width) (*11*). However, because *P′660P′* is often not observed, the 660 may be laterally variable in its reflective properties or the topography on the discontinuity may cause destructive interference of *P′660P′*. Complicating the picture are results from long-period *P*-to-*SV* conversions, which suggest that the 410 is sharp, but the 660 is a velocity and density gradient zone that is 20 to 30 km thick (*12*). Recent work (*13*) shows that a subducting slab below 410 km may destroy *P*-to-*SV* conversions from the 410 but not from the 660, thus demonstrating that the 660 is a stable feature in *P*-to-*SV* conversions.

Earlier studies (*14*) from mineral physics suggested that compositional change was necessary to explain the sharp *P′P′* reflections. Whether the 660 is a phase-change boundary or a compositional change has implications for whole mantle or two-layered convection (*14*, *15*), although hybrid models are possible and are supported by recent tomographic (*16*) and geodynamic modeling (*17*). We present here a velocity model, based on modeling of stacks of recent global seismic data, that may help to rectify the contradictions about the nature of the 660.

We used vertical-component, long-period (one sample per second) seismograms from the Global Seismic Network for 1990 through 1994 from earthquakes with a moment magnitude $M_w \geq 5.6$ recorded at epicentral distances between 60° and 180° (*18*). There were 31,792 seismograms in this data set, from 985 earthquakes, recorded at 132 stations. Of these seismograms, 20,216 were useful (no data errors, energy at *P* and *PP* arrival times in several frequency bands). We further culled the data set by selecting seismograms with signal-to-noise ratios (SNRs) of ≥2 and depths of ≤100 km (*19*). We analyzed these seismograms using software developed by Stammler (*20*).

Distance-time plots of the stacked observed seismograms (Fig. 1A) compared with stacked synthetic seismograms for the IASP91 model (*21*) (Fig. 1B) showed that the underside reflection *P660P* (*10*) (Fig. 1C) does not appear in the observations but does appear in the synthetics. To further improve the observational evidence, we transformed the distance-time wave field into the slowness-time domain. The results (Fig. 2, A to D) showed the reflection from 410 km (arriving 84 s before *PP* at the proper slowness) but nothing from 660 km. The reflection *P410P* arrived ~1 s earlier in the data than in IASP91. The amplitude ratio *P410P*/*PP* is ~2%, or about 60% of the ratio calculated for IASP91. The reflection *P660P* should arrive ~125 s before *PP* with a slowness about 0.3 s degree^{-1} less than that of *PP* and, according to IASP91, should have about the same amplitudes as *P410P*. The observed data showed no such phase. Slowness stacks calculated for different periods (1 to 50 s) and with varying subsets of the data remain essentially unchanged: they showed no evidence of the phase. These tests included seismograms with an SNR of ≥10 and from various distance ranges. To resolve whether the phase *P660P* might be observed regionally, we binned bounce points (calculated by tracing rays through IASP91) by tectonic region. A phase arriving at the predicted time of *P660P* was observed only from the region north of New Guinea and from Mexico; all other regions showed *P410P* but not *P660P*.

Observed transverse *SS*-wave seismograms (*4*) showed reflections from the 410 and 660 (Fig. 2C). Because both *P* and *S* signals (15-s and 30-s periods, respectively) have about the same wavelength, destructive interference of reflections from a 660 with topography cannot be the reason for our observation. To test the effect of topography, we varied the depth to the 660 in reflectivity *P*-wave seismograms randomly between 600 and 660 km. This effectively removed the short periods in the synthetics, but the longer periods (≥15 s) were unaffected. Thus, heterogeneity in the bounce-point region (*22*) cannot completely remove reflections from the 660. We also tried modeling the missing underside reflections with a gradient model (*12*), but, to minimize the amplitudes of the reflections, we found it necessary to extend the gradient over >100 km. The missing *P*-wave reflection from the 660 indicates that this discontinuity is predominantly a shear discontinuity.

Phases in the *P* and *PP* coda may also have reflection characteristics similar to those of the precursors to *PP* and might be used to confirm the results from *PP* precursors. Shearer (*3*) identified two phases in the *P* coda on the vertical component of stacks of global seismograms, *Pp410p* and *Pp660p* (*10*), appearing about 95 s and 140 s after the *P* wave, respectively. Our data also showed a phase at the arrival time of *Pp660p*. By chance, another phase, *Ps410p* (*10*), arrives at about the same time as *Pp660p*, irrespective of epicentral

GeoForschungsZentrum Potsdam, Telegrafenberg, D-14473 Potsdam, Germany.

*To whom correspondence should be addressed.
†Also at Freie Universität Berlin, Berlin, Germany.

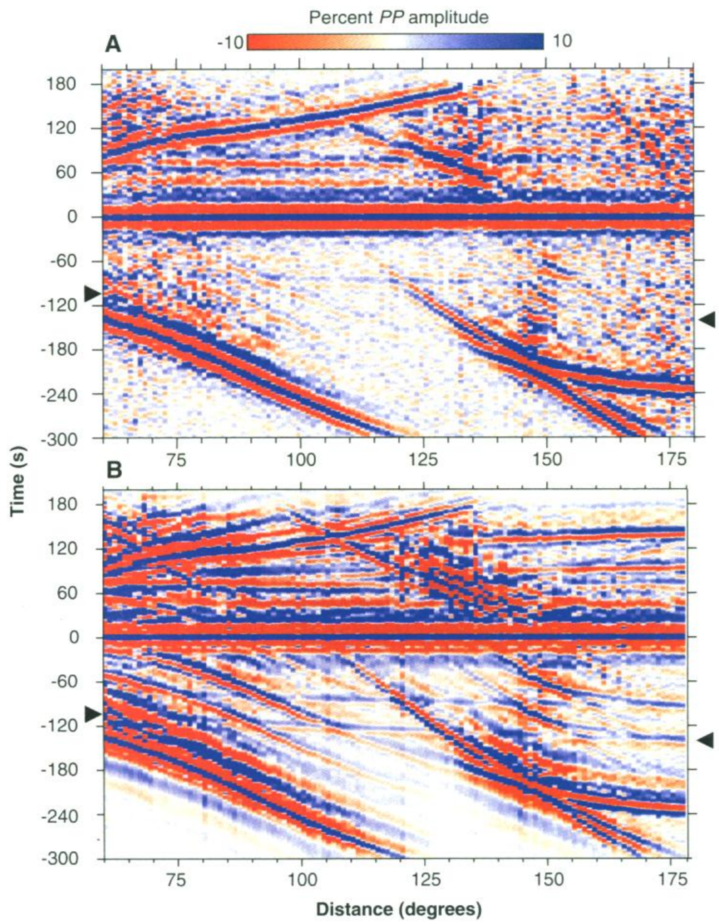

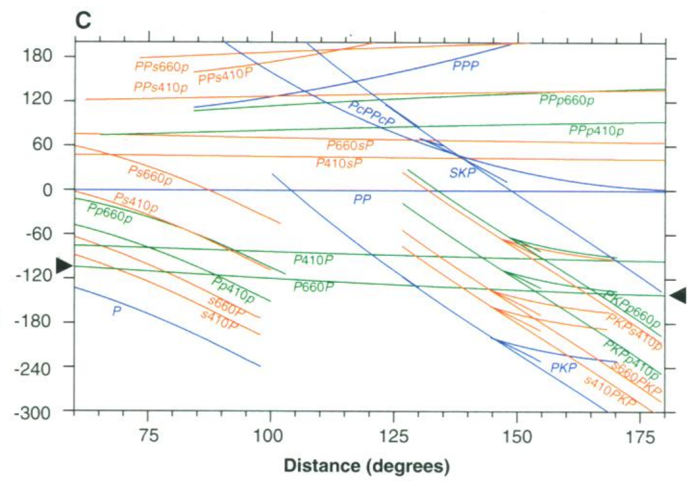

Fig. 1. (**A**) Distance-time plot of 7758 traces from observed seismograms stacked in bins of 1 s by 1°. The scale (at top) saturates at 10% of the *PP* amplitude. Arrowheads (left and right) mark the arrival time of *P660P*. Portrayal is done as in (*3*). *PcPPcP* appears as a large-amplitude phase in the *PP* coda, which contradicts (*3*). (**B**) Reflectivity synthetic seismograms (*35*) calculated for IASP91 and processed as in (A). In creating this image, 720 seismograms, calculated for 24 randomly chosen focal mechanisms from the Harvard Centroid Moment Tensor catalog with depths between 0 and 50 km, were used. (**C**) Travel-time curves calculated by tracing rays through IASP91. Blue lines are the main phases, green lines are multiples and underside reflections from the upper-mantle discontinuities, and red lines are the *SV*-to-*P* conversions from the discontinuities. Times for diffracted phases are not calculated. See (*3*) for a description of the labeled phases.

distance. Constructive interference of *Pp660p* and *Ps410p* in synthetics calculated for IASP91 (Fig. 3) nearly doubles the amplitude of *Pp660p* + *Ps410p* relative to that of *Pp410p*. The observed data, on the other hand, show that *Pp660p* + *Ps410p* and *Pp410p* have nearly the same amplitude. Forward modeling with synthetic seismograms suggests that the amplitude of *Pp660p* + *Ps410p*, and that of similar multiples in the PP coda, fits a model with a 2% *P*-wave velocity contrast at the 660. This modeling suggests that a pure *P* reflection (*P* incident, *P* reflected) does not exist in the global average from the 660, neither as *PP* precursors nor as secondary phases after *P* or *PP*.

We used several constraints to develop a velocity model for the 660. The amplitude of the underside *P*-reflection coefficient ($\acute{P}\grave{P}$) must be reduced while simultaneously maintaining large underside *S* reflections ($\acute{S}\grave{S}$) and *PS* conversions. We searched all possible *P* velocity (V_p), *S* velocity (V_s), and density (ρ) (*23*) combinations that minimize $\acute{P}\grave{P}$ while maximizing $\acute{S}\grave{S}$; V_s and ρ were bounded by the IASP91, respectively. We calculated reflection coefficients for two half-spaces in contact across the 660 (*24*). A small $\acute{P}\grave{P}$ reflection coefficient is the same as having no change in Lamé's constant λ and seismic parameter Φ. Lamé's constant λ relates stresses and strains in perpendicular directions (*25*), but the interpretation of λ in a multimineral system may be difficult. However, the constraint $\Delta\lambda = \Delta\Phi = 0$ decomposes the discontinuity to a change in shear modulus μ and ρ. Constraining V_s and ρ to IASP91 and AK135 values (*21*), respectively, results in our model, EK1 (*26*); it was necessary, however, to adjust ρ slightly to satisfy the constraint $\Delta\lambda = \Delta\Phi = 0$. This model (Fig. 4) has a discontinuity in V_p that is transparent to *P* waves with slownesses between 4.5 and 9.0 s degree^{-1} (Fig. 2D). It may prove easier to interpret $\Delta\Phi$ than $\Delta\lambda$ because it is available from laboratory experiments. Using our values of Φ and curves of $\sqrt{\Phi}$ versus depth for the pyrolite and piclogite models (*27*), we found that our value of Φ is more consistent with the piclogite model of the upper mantle (*8*), where the olivine component is 40% of the total composition. Note that the jump in the Poisson's ratio ν in EK1 is about eight times that in IASP91.

If there is a problem in the existing *P*-wave velocity model at the 660, why had it not been previously recognized? Travel-time curves from Gutenberg and Richter and from Jeffreys-Bullen (*28*) have phases that precede *PP*. The Jeffreys-Bullen travel-time chart from 1940 included a phase labeled *P400P* but did not include *P660P*. Shearer noted that "the bottomside reflection off the 410-km discontinuity (*P410P*) is visible between about 105° and 145°, although the corresponding 660-km phase (*P660P*) is not apparent. The absence of *P660P* is probably due to interference with other phases such as *PKP* and the topside *P* multiple *Pp660p*, although it is puzzling that at least a portion of *P660P* cannot be seen near 120°" (*3*, p. 18155). We tested this suggestion by slowness analysis of seismograms between 100° and 120°, a distance range relatively free of interfering phases (Fig. 1), and found that *P660P* does not appear.

Precursors to *P′P′* have been used to confirm the existence and sharpness of the 660, yet these data are different from the *PP* data in slowness and perhaps in frequency content. Then why are the results so different? As far as we know, there exists no comparable global study of *P′P′* that could answer this question. Precursors to *P′P′* are observed in some regions but not in others. Being short-period observations, they therefore might vary locally

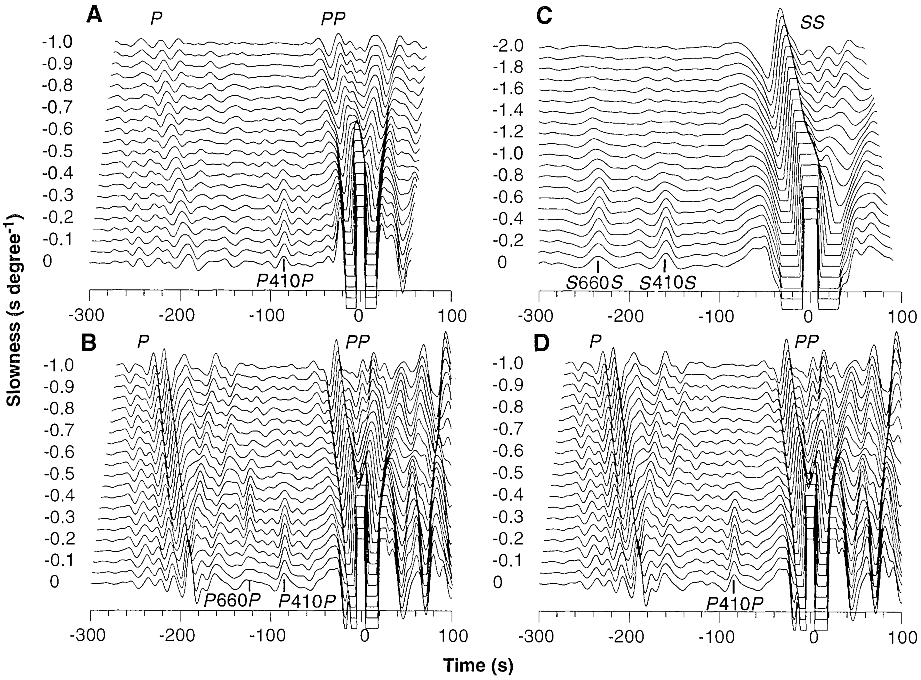

Fig. 2. (**A**) Slowness stack of the observed deconvolved seismograms with epicentral distances between 80° and 140° (6194 seismograms). Slownesses were calculated relative to *PP* for a reference distance of 110°. A greater negative slowness indicates a steeper incidence angle. Significant phases are marked. (**B**) Slowness stack of *PP*-wave synthetic seismograms calculated for IASP91. (**C**) Slowness stack of *SS*-transverse waves. Slownesses are relative to *SS* for a reference distance of 140°. (**D**) Slowness stack of *PP*-wave synthetic seismograms calculated for model EK1.

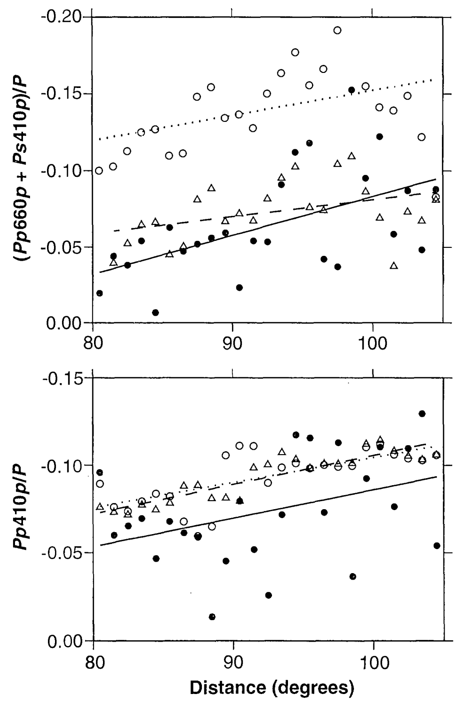

Fig. 3. Amplitude ratios as a function of epicentral distance for two phases in the *P* coda, from seismogram stacks in Fig. 1 with epicentral distances between 80° and 105° (other phases do not interfere at these distances). Straight lines are weighted least-squares fits. Observed data, solid circles and solid lines; IASP91, open circles and dotted lines; EK1, triangles and dashed lines.

more than do long-period data. We have some indication in our long-period data that some regions might have *PP* precursors from the 660. Furthermore, reflection coefficients (*24, 29*) and reflectivity modeling indicate that a near-vertical *P*-wave reflection (*P′P′*) from the 660 is produced by our model (~20% smaller in amplitude than predicted by IASP91). We suggest that the intermittent nature of *P′P′* precursors is caused by a smaller *P*-velocity jump combined with regional variations in the 660.

Wide-angle seismic data should show upper-mantle structure in the form of *P*-wave triplication between 15° and 30°. A clear triplication from the 410 and 660 was found under western North America and the Gulf of California (*30*). However, the triplication from the 660 is nearly always weaker than from the 410 or is sometimes not observed (*31*). Perhaps the best wide-angle data (controlled sources and very close station spacing) are from the Peaceful Nuclear Explosions in the former Soviet Union (*32*), which show an upper-mantle triplication from the 410, but a triplication from the 660 at about 24° epicentral distance is absent. The best-fit model to these data (*32*) has either a 50% *P*-wave velocity reduction at 660 or a 50-km gradient. This result is in agreement with reflection coefficients for wide-angle reflections with EK1. Wide-angle seismic data sometimes show a pronounced 660 and sometimes not, thus confirming the regional variability of the 660 and demonstrating that, in the global average, the 660 is a poor *P*-wave reflector. It is even transparent in the slowness range of 4.5 to 9.0 s degree^{-1}. The wide-angle studies are unevenly distributed globally and, moreover, are concentrated on the continents.

The EK1 model can be used to place limits on the relative abundances of minerals involved in the phase transformations at the 660. Earlier investigators (*8, 14*) recognized that a 660 involving only phase changes yielded a smaller than predicted *P*-wave velocity change as compared with PREM (*21*) and suggested that a change in chemical composition was needed. For our model, however, it is not necessary to introduce a compositional change to match the velocity structure. A model of mantle rheology (*33*) involving a phase change of the Sp and Gr components yields a velocity model similar to ours. An increase in the viscosity of the mantle across the 660 (*34*) has direct implications for convection models of the mantle and slab interaction with the lower mantle. Our model may support such a viscosity model.

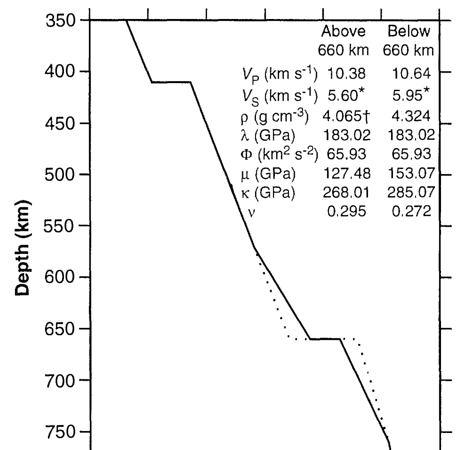

Fig. 4. *P*-wave velocity models EK1 (solid line) and IASP91 (dotted line). The inset gives the elastic parameters for EK1 (*, IASP91; †, AK135).

REFERENCES AND NOTES

1. L. P. Vinnik, *Phys. Earth Planet. Inter.* **15**, 39 (1977); K. Stammler *et al.*, *Geophys. Res. Lett.* **19**, 1563 (1992).
2. C. W. Wicks and M. A. Richards, *Geophys. J. Int.* **107**, 279 (1991); G. Bock and R. Kind, *ibid.*, p. 117.
3. P. M. Shearer, *J. Geophys. Res.* **96**, 18147 (1991).

4. J. Gossler and R. Kind, *Earth Planet. Sci. Lett.* **138**, 1 (1996).
5. P. M. Shearer, *Geophys. J. Int.* **115**, 878 (1993).
6. N. Wajeman, *Geophys. Res. Lett.* **15**, 669 (1988).
7. E. Ito and E. Takahashi, *J. Geophys. Res.* **94**, 10637 (1989).
8. T. Duffy and D. L. Anderson, *ibid.*, p. 1895.
9. T. Irifune, *Phys. Earth Planet. Inter.* **45**, 324 (1987).
10. *PP* is a *P* wave that reflects once from Earth's surface. *P′P′* (*PKPPKP*) is like *PP* but travels through the core. *PzP* are underside reflections, where *z* is the depth of the reflection (for example, *P660P* is a *P* wave reflected from a depth of 660 km). *Pdzd* are topside reflections where *d* is either *p* or *s* (for example, *Ps660p* is a *P* wave with a source- or receiver-side *S-P* reflection-conversion).
11. H. M. Benz and J. E. Vidale, *Nature* **365**, 147 (1993).
12. N. Petersen *et al.*, *Geophys. Res. Lett.* **20**, 859 (1993); M. G. Bostock, *ibid.* **23**, 1593 (1996).
13. L. Vinnik, G. Kosarev, N. Petersen, *ibid.*, p. 1485.
14. A. C. Lees, M. S. T. Bukowinski, R. Jeanloz, *J. Geophys. Res.* **88**, 8145 (1983).
15. U. R. Christensen and D. A. Yuen, *ibid.* **89**, 4389 (1984).
16. R. van der Hilst, E. R. Engdahl, W. Spakman, *Geophys. J. Int.* **115**, 264 (1993).
17. U. Christensen, *Earth Planet. Sci. Lett.* **140**, 27 (1996); H.-P. Bunge, M. A. Richards, J. R. Baumgardner, *Nature* **379**, 436 (1996); P. J. Tackley, D. J. Stevenson, G. A. Glatzmaier, G. Schubert, *J. Geophys. Res.* **99**, 15877 (1994).
18. The data were provided by IRIS-Seattle (Incorporated Research Institutions for Seismology) as FARM (fast archive recovery method) data volumes.
19. We calculated the SNR from the peak-to-peak amplitude (PTPA) 65 to 5 s before the predicted *PP* arrival time versus the PTPA from the *PP* time to 60 s after, using the band-pass–filtered seismograms (10 to 50 s).
20. K. Stammler, *Comput. Geosci.* **19**, 135 (1993). The data were detrended and filtered with a causal three-pole bandpass filter between 3 and 50 s before deconvolution and filtered again with a three-pole acausal bandpass filter between 10 and 50 s to shift the weighting toward longer periods. The acausal filter produced symmetric side lobes, which appeared in the synthetics (Fig. 1B, appearing ~60 s before *P* and *PKP*) but not in the data. The stacking procedure apparently canceled out this effect when applied to the data because of the sheer number of events. The *PP* phase was deconvolved from the entire seismogram to account for varying source-time histories and radiation patterns. To enhance the amplitude of the precursors to *PP*, we aligned the seismograms on the resulting spike and slant-stacked (stacking along a travel-time curve) to obtain the slownesses (inverse of apparent velocity) of the *PP* phase and its precursors (*1*).
21. International Association of Seismology and the Physics of the Earth's Interior [B. L. N. Kennett and E. R. Engdahl, *Geophys. J. Int.* **105**, 429 (1991)]. Attenuation Q^{-1} is from the Preliminary Reference Earth Model [A. M. Dziewonski and D. L. Anderson, *Phys. Earth Planet. Inter.* **25**, 297 (1981)]. Density is from AK135 [B. L. N. Kennett, E. R. Engdahl, R. Buland, *Geophys. J. Int.* **122**, 108 (1995)].
22. F. Neele, H. de Regt, J. VanDecar, in preparation.
23. $V_p = \sqrt{(\lambda + 2\mu)/\rho} = \sqrt{(\kappa + 4\mu/3)/\rho}$, where λ and μ are the Lamé parameters (μ is also known as the shear modulus) and κ is the bulk modulus:
$$\Phi = (\lambda + 2\mu/3)/\rho = \kappa/\rho$$
24. K. Aki and P. Richards, *Quantitative Seismology: Theory and Methods* (Freeman, San Francisco, 1980), vol. 1.
25. J. C. Jaeger, *Elasticity, Fracture, and Flow: With Engineering and Geological Applications* (Chapman and Hall, London, 1969).
26. For waves with a slowness of 7 s degree^{-1} (*PP* slowness for a distance of 120°), a model for which V_p is constant but V_s and ρ change produces a small $\dot{P}\dot{P}$, whereas a model in which V_p and ρ are constant but V_s changes produces a large but negative $\dot{P}\dot{P}$ as compared with IASP91. $\dot{S}\dot{S}$ is significant only when there is a jump in V_s and ρ.
27. J. Ita and L. Stixrude, *J. Geophys. Res.* **97**, 6849 (1992).
28. K. E. Bullen and B. A. Bolt, *An Introduction to the Theory of Seismology* (Cambridge Univ. Press, Cambridge, 1987).
29. R. Kind, *J. Geophys.* **42**, 191 (1976).
30. S. P. Grand and D. V. Helmberger, *Geophys. J. R. Astron. Soc.* **76**, 399 (1984); M. C. Walck, *ibid.*, p. 697; L. E. Jones, J. Mori, D. V. Helmberger, *J. Geophys. Res.* **97**, 8765 (1992).
31. J. R. Bowman and B. L. N. Kennett, *Geophys. J. Int.* **101**, 411 (1990).
32. T. Ryberg *et al.*, *Ann. Geophys.* (abstract) (1996), p. C68.
33. P. Vacher, A. Mocquet, C. Sotin, *ibid.*, p. C41.
34. B. H. Hager and M. A. Richards, *Philos. Trans. R. Soc. London Ser. A* **328**, 309 (1989); A. M. Forte, A. M. Dziewonski, R. J. O'Connell, *Science* **268**, 386 (1995).
35. R. Kind, *J. Geophys.* **45**, 373 (1979).
36. We thank G. Bock, J. Gossler, W. Hanka, F. Krüger, P. Richards, T. Ryberg, C. Scholz, and S. Sobolev for helpful discussions and reviews. We thank IRIS-Seattle for the FARM tapes and contributing stations from the Federation of Digital Seismic Networks. K. Stammler, R. Benson, and T. McSweeny supplied software. Supported by the Deutsche Forschungsgemeinschaft.

23 May 1996; accepted 16 September 1996

Organic Glasses: A New Class of Photorefractive Materials

P. M. Lundquist, R. Wortmann,* C. Geletneky,† R. J. Twieg,‡ M. Jurich, V. Y. Lee, C. R. Moylan, D. M. Burland‡

The performance of amorphous organic photorefractive (PR) materials in applications such as optical data storage is generally limited by the concentration of active molecules (chromophores) that can be incorporated into the host without forming a crystalline material with poor optical quality. In polymeric PR systems described previously, performance has been limited by the necessity of devoting a large fraction of the material to inert polymer and plasticizing components in order to ensure compositional stability. A new class of organic PR materials composed of multifunctional glass-forming organic chromophores is described that have long-term stability and greatly improved PR properties.

The PR effect may be defined as the spatial modulation of a material's refractive index *n* in response to an optically induced charge distribution. The spatial index modulation may be out of phase with the spatial modulation of the original optical excitation, and this phase shift can induce an exchange of energy between laser beams, which leads to a variety of applications including optical correlators, beam-fanning intensity limiters, and novelty filters (*1*). Photorefractive materials have also been considered for use as reversible recording media in holographic optical data storage. In addition to large changes in *n* per unit photon absorbed, most applications require PR media with high optical clarity and minimal light-scattering levels. We report here a new type of PR system based on amorphous organic glasses (*2*) with substantial improvements in PR and sample-quality properties.

The PR effect was first observed in a $LiNbO_3$ crystal more than 30 years ago (*3*). Polymeric PR materials were initially described in 1991 (*4*). In the relatively brief intervening period, their performance has improved dramatically (*5, 6*) to the point where important properties, such as maximum *n* modulation (Δn) and two-beam coupling (2BC) gain (Γ), actually equal or exceed those of their inorganic counterparts (*7*). The features required for PR behavior (photocharge generation, photoconductivity, charge trapping, and nonlinear or birefringent optical response) are usually provided by separate components, each of which can be dissolved as a guest in the polymer host or chemically attached to the polymer. Several of the most promising polymeric PR materials containing a charge transport polymer host are designed in this way (*8, 9*). The largest Δn and Γ previously reported were measured in a mixture of the nonlinear optical chromophore 2,5-dimethyl-4-*p*-nitrophenylazoanisole (DMNPAA) doped into a polyvinylcarbazole (PVK) host polymer with a plasticizer (9-ethylcarbazole, ECZ) and a small quantity of 2,4,7-trinitro-9-fluorenone (TNF) added as a charge-generating photosensitizer (*10*). Unfortunately, the high concentration (up to 50 weight %) of DMNPAA required to produce the large Δn results in a metastable material system in which the chromophore crystallizes out over time, a process that seriously com-

Almaden Research Center, IBM Research Division, 650 Harry Road, San Jose, CA 95120-6099, USA.

*Present address: Institut für Physikalische Chemie, Johannes Gutenberg-Universität, Jakob Welder-Weg 11, 55099 Mainz, Germany.
†Present address: FB Chemie der Philipps-Universität, Hans-Meerwein-Strasse, 35032 Marburg, Germany.
‡To whom correspondence should be addressed.